Seismic performance assessment of steel frame infilled with prefabricated wood shear walls

Zheng Li [a,*], Minjuan He [a], Xijun Wang [a], Minghao Li [b]

[a] *Department of Structural Engineering, Tongji Univ., 1239 Siping Rd., Shanghai 200092, China*
[b] *Department of Civil & Natural Resources Engineering, Univ. of Canterbury, Private Bag 4800 Christchurch, New Zealand*

ARTICLE INFO

ABSTRACT

Steel-timber hybrid structural systems offer a modern solution for building multi-story structures with more environmentally-friendly features. This paper presents a comprehensive seismic performance assessment for a kind of multi-story steel-timber hybrid structure. In such a hybrid structure, steel moment resisting frames are infilled with prefabricated light wood frame shear walls to serve as the lateral load resisting system (LLRS). In this paper, drift-based performance objectives under various seismic hazard levels were proposed based on experimental observations. Then, a numerical model of the hybrid structure considering damage accumulation and stiffness degradation was developed and verified by experimental results, and nonlinear time-history analyses were conducted to establish a database of seismic responses. The numerical results further serve as a technical basis for estimating the structure's fundamental period and evaluating post-yielding behavior and failure probabilities of the hybrid structure under various seismic hazard levels. A load sharing parameter was defined to describe the wall-frame lateral force distribution, and a formula was proposed and calibrated by the time-history analytical results to estimate the load sharing parameter. Moreover, earthquake-induced non-structural damage and residual deformation were also evaluated, showing that if designed properly, desirable seismic performance with acceptable repair effort can be obtained for the proposed steel-timber hybrid structural system.

© 2017 Elsevier Ltd. All rights reserved.

1. Introduction

In recent devastating earthquakes around the world, many buildings suffered severe damage, leading to huge social and economic losses. The 2008 Wenchuan earthquake in China, with a magnitude of Mw 8.0, caused approximately $130 billion USD in property losses [1]. The post-earthquake survey revealed that casualties were primarily caused by the collapse of masonry or concrete buildings with large seismic mass and poor construction quality. The 2011 Christchurch earthquake in New Zealand, with a magnitude of Mw 6.3, caused 185 deaths, and the central city of Christchurch was badly affected with severe damage to buildings and infrastructures that were already weakened by the preceding Canterbury earthquake, with a magnitude of Mw 7.1, in 2010 [2]. Experiences from past major earthquakes demonstrated that relatively lightweight timber or timber-based buildings kept more people safe. To provide an alternative for multi-story building systems in seismic-prone zones, a steel-timber hybrid structure was proposed by He et al. [3] and Li et al. [4]. In such structures, the steel moment-resisting frames

are infilled with prefabricated light wood frame shear walls to serve as the lateral load resisting system (LLRS), and the diaphragms are composed of C-shaped steel joints and dimension lumber decking. The weight of the proposed structural system is largely reduced with the application of wood assemblies; thus, the seismic action on the entire building is also considerably reduced.

With the urgent need for building industrialization and the use of more environmentally-friendly materials, such as wood, in building construction, multi-story steel-timber hybrid structural systems have attracted much research attention in the past decade. The seismic performance of a steel-timber hybrid system, where cross-laminated timber (CLT) panels are used as infill walls in a steel moment-resisting frame, was analytically investigated by Tesfamariam et al. [5]. Seismic vulnerability assessments were conducted on the hybrid system, and a parametric study was carried out with a 1-story, 1-bay model using pushover analysis to investigate the effects of CLT panel thickness on the behavior of the LLRS. Subsequently, a ductility factor of 2.5 and an over-strength factor of 1.25 were recommended for the steel frame infilled with CLT panels [6]. Zhang et al. [7] investigated the ductility of a 12-story steel-timber hybrid structure, where CLT panels serve as shear walls and are connected to each other through steel beams, and the potential ductility factor for the prototype structure was calibrated based on nonlinear time-history analyses.

* Corresponding author.
E-mail addresses: zhengli@tongji.edu.cn (Z. Li), hemj@tongji.edu.cn (M. He), 1530552@tongji.edu.cn (X. Wang), minghao.li@canterbury.ac.nz (M. Li).

In this study, the proposed structural system utilizes light wood frame shear walls as infills, instead of CLT panels, to provide lateral resistance. CLT is a solid panel product with a crosswise layup of wood boards bonded with adhesives. Although CLT has a considerably higher in-plane stiffness compared to a light frame wood system, high production costs may limit its wide application, especially in a country with limited forestry resources, such as China. Thus, with a relatively low production cost, light wood frame shear walls can provide a more cost-effective solution for multi-story steel-timber hybrid buildings. In the proposed structural system, the LLRS is composed of a steel moment-resisting frame and infill light wood frame shear wall. For a shear wall-frame interactive system, it is noted from ASCE 7–10 [8] that the shear strength of the shear walls shall be at least 75% of the design story shear at each story. Accordingly, the frames of the shear wall-frame interactive system shall be capable of resisting at least 25% of the design story shear in each story. However, previous experimental results from He et al. [3] demonstrated that the light wood frame shear walls are normally insufficient to resist 75% of the design story shear in a steel-timber hybrid structure. Thus, the evaluation of the load sharing mechanism between the steel frame and the infill wood shear wall appears necessary to reach a more comprehensive understanding of the structure's seismic behavior. This paper presents a seismic performance assessment of the multi-story steel-timber hybrid structure. A nonlinear numerical model considering damage accumulation and stiffness degradation was created and verified by test results, and the seismic performance of the proposed hybrid structure was evaluated with performance-based approaches.

2. Basic design considerations

The basic unit of the proposed steel-timber hybrid structure is shown in Fig. 1. The steel frame was assembled with hot rolled H-section steel members with a rigid beam to column connection, and prefabricated light wood frame shear walls were installed as infill walls. As a modularized structural system, light frame wood shear walls consist of a wood frame, made of dimension lumber, and sheathing panels made of oriented strand board (OSB) or plywood board, and the sheathing panels are connected to the wood frame by nails. The wood frame is normally fabricated with lumber with the dimensions 2 × 4 (i.e., 38 mm × 89 mm cross section) or 2 × 6 (i.e., 38 mm × 140 mm in cross section), and the distance between adjacent lumber is normally assigned as 305 mm, 406 mm, or 610 mm. The thickness of sheathing panels can be 9.5 mm, 12 mm, or 14.7 mm. The stiffness and strength of a light frame wood shear wall is primarily determined by the layouts of the sheathing-to-framing nailed connections (i.e., nail spacing, nail size). Bolted connections were used to connect the boundary elements of the infill wall to the steel frame. The bolted
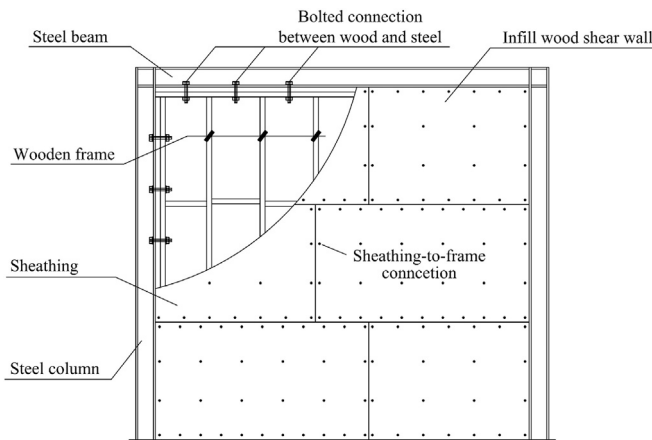
connections transfer shear force between the steel fame and the infill wall, ensuring that the infill wall and the steel frame can simultaneously deform and resist lateral loads. The steel moment-resisting frame, combined with the infill wall, act as dual LLRS. When subjected to shear force, the lateral resistance of a light wood frame shear wall comes from the combination of shear resistance from the numerous nailed sheathing-to-framing connections, and it is quite difficult to accurately predict the lateral resistance of a light wood frame shear wall with theoretical calculations. Previous studies [9–10] demonstrated that inter-story drift could be correlated with the lateral load resisting performance of light wood frame shear walls in a straightforward calculation. Therefore, hybrid LLRS can be designed with performance-based approaches. This section provides a preliminary design procedure for the proposed steel-timber hybrid LLRS, which mainly follows the performance-based design procedure recommended by Goel and Chao [11] for steel plate shear walls. The design considered a pre-selected preferred yield mechanism, as shown in Fig. 2. This yield mechanism consists of the formation of plastic hinges at both beam ends and column bases, and the "yielding" of the infill wall. Since the pushover response of the wood shear wall exhibits a high nonlinear property, the "yielding" of a wood shear wall can be considered as the point on the pushover curve corresponding to 40% of ultimate capacity (i.e., 0.4 P_{peak}). In accordance with the energy balance concept, the inelastic energy demand is equal to the inelastic work performed internally in a structural system. The total strain energy demand of inelastic single-degree-of-freedom (SDOF) system can be predicted by.

$$E_e + E_p = \gamma \cdot \frac{1}{2} M S_v^2 = \frac{1}{2} \gamma M \left(\frac{T_1}{2\pi} \cdot S_a g \right)^2 \tag{1}$$

where E_e is the elastic strain energy demand; E_p is the plastic strain energy demand; γ is the energy modification factor; M is the seismic mass; S_v is the spectral velocity corresponding to the fundamental period of the structure T_1; S_a is the spectral acceleration; and g is the acceleration of gravity. Assuming that the entire structure is a SDOF system, the elastic energy E_e can be estimated by Eq. (2) according to Akiyama [12]:

$$E_e = \frac{1}{2} M \left(\frac{T_1}{2\pi} \cdot \frac{V_b}{G} \cdot g \right)^2 \tag{2}$$

where V_b is the base shear, and G is the seismic weight of the structure. The energy modification factor can be determined by.

$$\gamma = \frac{2\mu_t - 1}{R_u^2} \tag{3}$$

where μ_t is the target displacement ductility ratio and is equal to Δ_t / Δ_y. Then, Δ_t is the target lateral displacement, and Δ_y is the yield lateral displacement. R_u is the ductility-based reduction factor, equal to Δ_{eu} / Δ_y, and Δ_{eu} is the elastic target lateral displacement. Considering the selected yield mechanism, the structure can be idealized as an elastic perfectly plastic equivalent SDOF system, and the plastic energy E_p is calculated by as.

$$E_p = \frac{G T_1^2 g}{8\pi^2} \cdot \left[\gamma S_a^2 - \left(\frac{V_{by}}{G} \right)^2 \right] \tag{4}$$

where V_{by} is the yield base shear of the structure. The plastic energy demand is equal to the work performed by the lateral force under inelastic deformation as.

$$E_p = \sum F_i H_i \cdot \theta_p = V_{by} \cdot \sum \eta_i H_i \cdot \theta_p \tag{5}$$

where F_i and H_i are the lateral force and height of the ith story; θ_p is plastic inter-story drift and equal to $\theta_t - \theta_y$; θ_t is the target inter-story drift, and θ_y is the yield inter-story drift; and η_i is the lateral force distribution

Fig. 1. Basic unit of steel-timber hybrid structure.
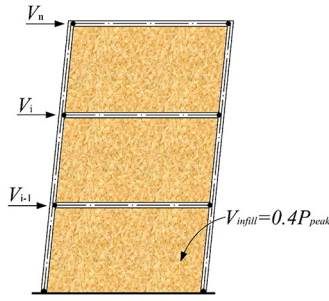
Fig. 2. Yield mechanism of steel-timber hybrid LLRS.

Fig. 3. Flowchart of designing steel-timber hybrid LLRS.

factor of the ith story. Substituting Eq. (4) into Eq. (5) generates a quadratic equation, and its solution gives.

$$V_{by} = G \cdot \left(\frac{-\xi + \sqrt{\xi^2 + 4\gamma S_s^2}}{2} \right), \quad \text{and} \quad \xi = \sum \eta_i H_i \cdot \frac{8\theta_p \pi^2}{T_1^2 g} \qquad (6)$$

The lateral force distributions given in design codes are primarily based on the elastic response of structures. The lateral force distributions during a nonlinear response may not be represented by code that is defined as lateral force distributions, and this can lead to inaccurate predictions of lateral force demands. To account for structural inelastic behavior during major earthquakes, the force distribution based on the inelastic state of structure can be considered as recommended by Chao et al. [13]. The required yield base shear at the ith story, V_i, and that at the top story, V_n, can be determined by Eqs. (7) and (8):

$$V_i = \left(\sum_{j=i}^{n} G_i H_i \Big/ \sum_{j=1}^{n} G_i H_i \right)^{0.75 T_1^{-0.2}} \cdot V_{by} \qquad (7)$$

$$V_n = \left(G_n H_n \Big/ \sum_{j=1}^{n} G_i H_i \right)^{0.75 T_1^{-0.2}} \cdot V_{by} \qquad (8)$$

where G_i and G_n are the seismic weight of the ith and the top story, respectively; H_i and H_n are the height of the ith and the top story, respectively. In the performance-based design for steel plate shear walls, it is normally assumed that the steel plate carries full story shear [14]. However, for the steel-timber hybrid LLRS, the shear resistance of the wood shear wall is normally insufficient to resist full-story shear, and the contribution of lateral resistance from the steel frame should be considered. Thus, it is proposed that the obtained story shear from Eqs. (7) and (8) should be further divided according to a load sharing ratio κ. Then, the infill wood shear wall is designed to carried story shear κV_i, and the steel frame is designed to meet $(1-\kappa)V_i$. Fig. 3 demonstrates the proposed lateral force design flowchart for the steel-timber hybrid LLRS.

For the proposed design procedure, the drift target should be defined, and the fundamental period of the structure should be estimated. More importantly, a proper load sharing parameter κ should be determined. However, no technical basis is available for estimating the structural period of the steel-timber hybrid system, and research on the wall-frame load sharing mechanism and post-yielding behavior of multi-story steel-timber hybrid structure is also quite insufficient. To shed some light on these topics, an investigation into the nonlinear seismic performance of the steel-timber hybrid structure was carried out in this study.

3. Prototype structure configuration

In this section, several prototype structures were provided, and the nonlinear seismic performance of these structures served as benchmark
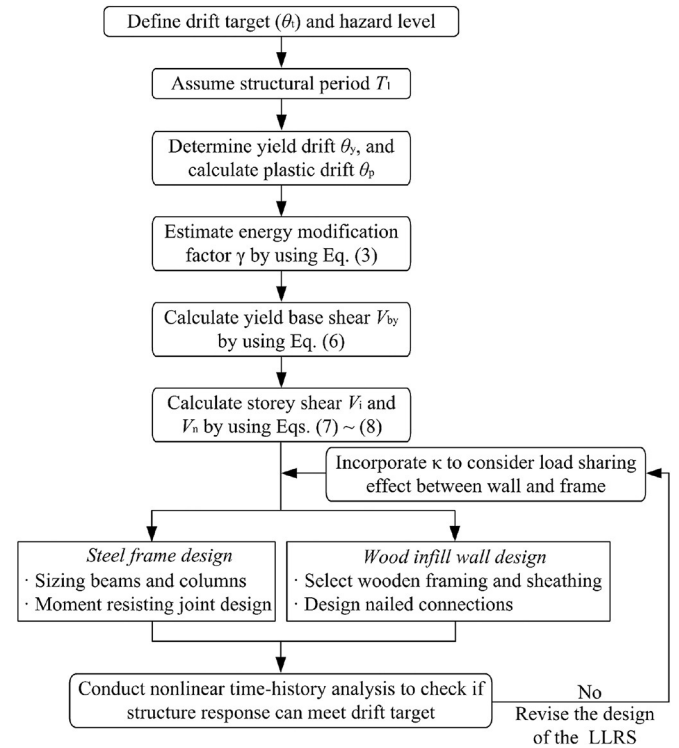
to provide recommendations on the design procedure (e.g., which load sharing parameter κ should be adopted). The prototype structure configuration mainly consisted of two parameters, one was building height and the other was the lateral wall-to-frame stiffness ratio. The building heights chosen were 3-story, 6-story, and 9-story. According to previous studies in Ref. [3], the lateral wall-to-frame stiffness ratio, λ, was an important parameter affecting the load resisting behavior of the LLRS, where λ is defined as.

$$\lambda = k_{wood}/k_{steel} \qquad (9)$$

where k_{wood} is the lateral stiffness of the infill wood shear wall and can be determined as $0.4P_{peak}/\Delta_{in\ fill}$, where P_{peak} (kN) is the peak load resisted by the infill wood shear wall on the backbone curve; and $\Delta_{in\ fill}$ (mm) is the lateral displacement of the infill wall at $0.4P_{peak}$. Then, k_{steel} is the elastic lateral stiffness of the steel moment-resisting frame and can be determined by frame analysis or finite element modeling. Previous studies revealed that for practical designs of the steel-timber hybrid LLRS, λ normally ranged from 1.0 to 3.0. λ had a significant influence on the wall-frame load sharing mechanism, energy dissipation capacity, and ductility of the LLRS. If LLRS adopted a large λ, the infill wood shear wall tended to resist a large portion of the lateral load. Accordingly, the ductility of the LLRS was likely to decrease due to the stiffness and strength degradation of the infill wood shear wall. In this study, three different lateral stiffness ratios (i.e., $\lambda = 1:1$, 2:1, and 3:1) were considered for each building height, resulting in nine prototype structure designs.

Identical floor plans were adopted for all prototype structures, as shown in Fig. 4, which also provides the elevations of LLRSs. The story height was taken as 3.3 m. The floor live load was taken as 2.5 kN/m² for office buildings, and 0.5 kN/m² was taken as the roof live load. The dead loads for the floors and roofs were 4.0 kN/m² and 1.8 kN/m², respectively. Mild carbon structural steel Q235B, with a yielding strength of 235 MPa and modulus of elasticity of 206 GPa, was used for the steel frame members. For each building height, the steel frame members were sized according to basic requirements in Chinese Code for Design
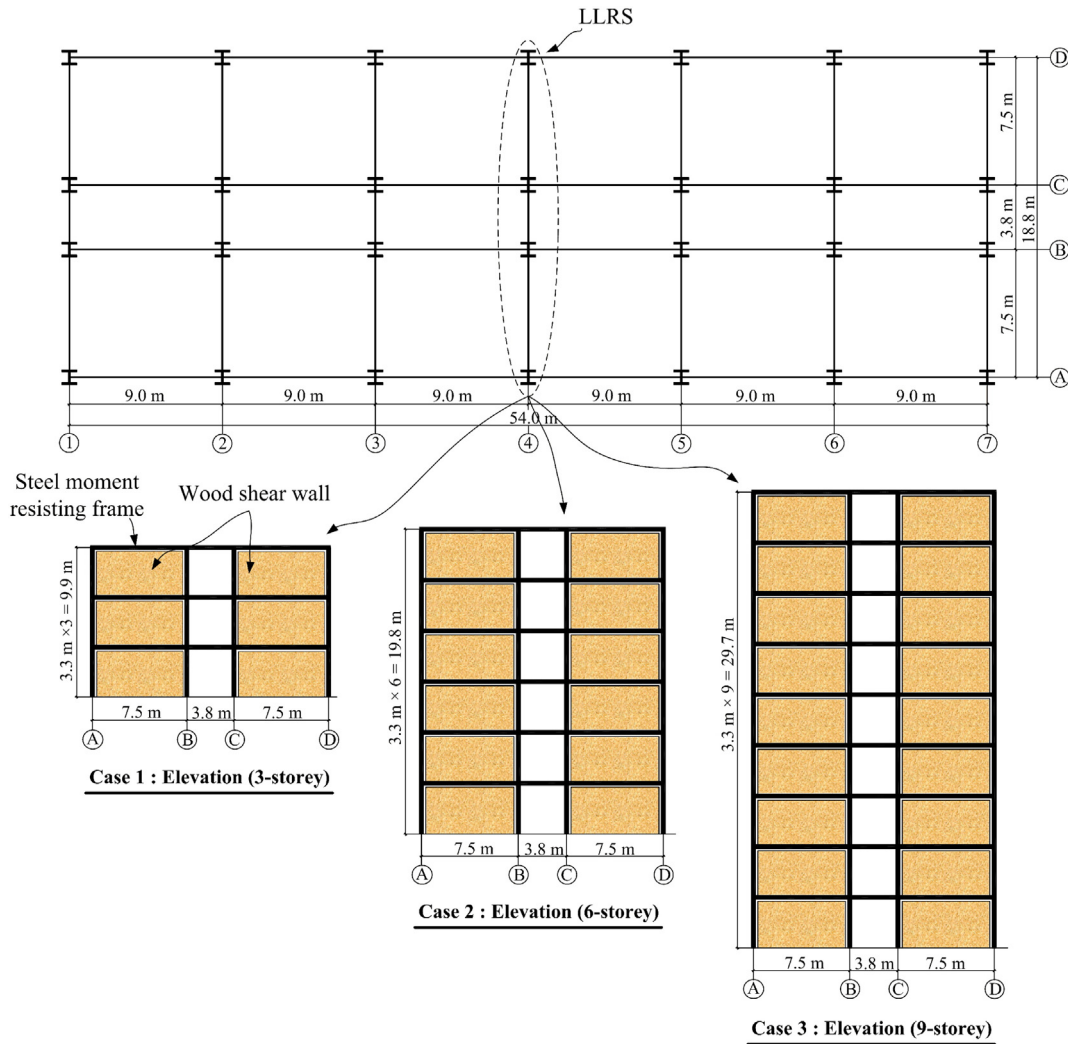
Fig. 4. Configuration of the prototype structures.

of Steel Structures (CCDSS) [15] and Chinese Code for Seismic Design of Buildings (CCSDB) [16], and the lateral stiffness in each story provided by the steel moment-resisting frame was obtained from a finite element based pushover analysis. The sections of steel members are summarized in Table 1. The stiffness of the infill wood shear wall in each story was determined according to the lateral stiffness ratio λ, which equaled 1.0, 2.0, or 3.0. Then, the infill wood shear wall was designed according to the provisions in the Chinese Code for Design of Timber Structures (CCDTS) [17]. Specifically, the stiffness of the light frame wood shear wall was designed as λ times the stiffness of the steel frame, and the

required stiffness of the light frame wood shear wall was primarily achieved by adjusting the layouts of sheathing-to-framing nailed connections, such as using smaller nail spacing for stiffer walls. As mentioned before, the stiffness of the wood shear wall can be calculated as the secant stiffness corresponding to the 40% of the ultimate load resisting capacity. For the prototype structures, the framing of the wood shear walls was fabricated with 2 × 6 dimension lumber (i.e., 38 mm × 140 mm cross section) with a spacing of 305 mm between adjacent members, and 12d common nails, which are confirmed to ASTM F1667 [18], with 82 mm length and 3.8 mm diameter were

Table 1
Sections of steel frame members*.

Building height	Storey no.	Column	Beam (external)	Beam (internal)
3-Storey	1	H-250 × 250 × 9 × 14	H-350 × 175 × 7 × 11	H-150 × 100 × 6 × 9
	2	H-200 × 200 × 8 × 12	H-350 × 175 × 7 × 11	H-150 × 100 × 6 × 9
	3	H-200 × 200 × 8 × 12	H-250 × 175 × 7 × 11	H-150 × 100 × 6 × 9
6-Storey	1, 2, 3	H-300 × 300 × 12 × 12	H-350 × 175 × 7 × 11	H-150 × 100 × 6 × 9
	4, 5	H-250 × 250 × 9 × 14	H-350 × 175 × 7 × 11	H-150 × 100 × 6 × 9
	6	H-250 × 250 × 9 × 14	H-250 × 175 × 7 × 11	H-150 × 100 × 6 × 9
9-Storey	1, 2, 3	H-300 × 300 × 15 × 15	H-350 × 175 × 7 × 11	H-150 × 100 × 6 × 9
	4, 5, 6	H-250 × 250 × 14 × 14	H-350 × 175 × 7 × 11	H-150 × 100 × 6 × 9
	7, 8	H-200 × 200 × 12 × 12	H-350 × 175 × 7 × 11	H-150 × 100 × 6 × 9
	9	H-200 × 200 × 12 × 12	H-320 × 150 × 6.5 × 9	H-150 × 100 × 6 × 9

*Note: The members are all hot rolled H-section steel members. H-$a \times b \times c \times d$ indicates the section has a height of a and a width of b. The web thickness is c, and the flange thickness is d.

Table 2
Configurations of the infill wood shear walls for the prototype structures.

Building height	Storey no.	Sheathing type	Nail spacing and sheathing pattern*		
			$\lambda = 1$	$\lambda = 2$	$\lambda = 3$
3-Storey	1	12 mm OSB	150/300 (S)	75/150 (S)	75/150 (D)
	2	9.5 mm OSB	100/200 (S)	50/100 (S)	50/100 (D)
	3	9.5 mm OSB	150/300 (S)	75/150 (S)	75/150 (D)
6-Storey	1, 2, 3	12 mm OSB	100/200 (S)	50/100 (S)	50/100 (D)
	4, 5	12 mm OSB	150/300 (S)	75/150 (S)	75/150 (D)
	6	9.5 mm OSB	100/200 (S)	50/100 (S)	50/100 (D)
9-Storey	1, 2, 3	14.7 mm OSB	100/200 (S)	50/100 (S)	50/100 (D)
	4, 5, 6	14.7 mm OSB	150/300 (S)	75/150 (S)	75/150 (D)
	7, 8	12 mm OSB	150/300 (S)	75/150 (S)	75/150 (D)
	9	9.5 mm OSB	100/200 (S)	50/100 (S)	50/100 (D)

*Note: 150/300 (S or D) indicates the sheathing panels are attached to the wood frame members with nails spacing at 150 mm on center along the panel edges, and spacing at 300 mm on center along the intermediate supports. S (or D) indicates the wood frame is sheathed with single sided (or double sided) OSB panels.

used as sheathing-to-framing fasteners. Other design information of the light frame wood shear walls for the prototype structures are listed in Table 2. Bolted connections were used to connect the infill wood shear wall to the steel frame. In accordance with Li et al. [19], these bolted connections were designed to have sufficient stiffness and strength so that the shear force could be effectively transferred between steel and wood, allowing the steel frame and the infill wood wall to resist lateral loads as a dual system.

4. Finite element model

4.1. General description

A nonlinear finite element (FE) model for the proposed structure was developed using the OpenSees framework [20]. The steel frame was modeled by displacement-based beam-column element (i.e., dispBeamColumn) with a uniaxial bilinear steel material with a kinematic hardening property (i.e., steel01). The yield strength and modulus of elasticity of steel were 235 MPa and 206 GPa, respectively. The steel sections were meshed into fiber sections and aggregated with shear and torsional stiffness. To increase the accuracy of the modeling, five-point Gauss-Lobatto integration was assigned with the steel column and beam elements.

4.2. Wood infill wall modeling

The hysteresis behavior of the light wood frame shear wall featured a significant pinching effect due to the strength/stiffness degradation. In previous studies, a few hysteretic models were developed and integrated with a user defined element in commercially available software, such as ABAQUS, to model the behavior of wood shear walls as multi-linear spring elements [21–22]. To increase the robustness of the numerical model, a mechanical-based hysteretic element for wood shear walls within ABAQUS was also developed, and the user-defined element was further used to simulate the seismic response of timber-steel hybrid structures [23]. However, the compiling of user defined element normally requires significant time and effort, which makes such a modeling approach too difficult to be used by others. OpenSees has become a preferred tool in earthquake engineering, with a complete element library. In this study, the hysteresis behavior of light wood frame shear walls was modeled by the "twoNodeLink" element with the "Pinching4" uniaxial material, which was developed for pinched systems within the OpenSees framework. As long as the hysteresis of a wood shear wall was obtained from an experiment or detailed numerical modeling, the calibration of the "Pinching4" material parameters could be easily performed by the regression algorithm.

4.3. Model verification

A 1-story 1-bay FE model, as shown in Fig. 5, was established and verified by test results presented in He et al. [3]. The model predictions
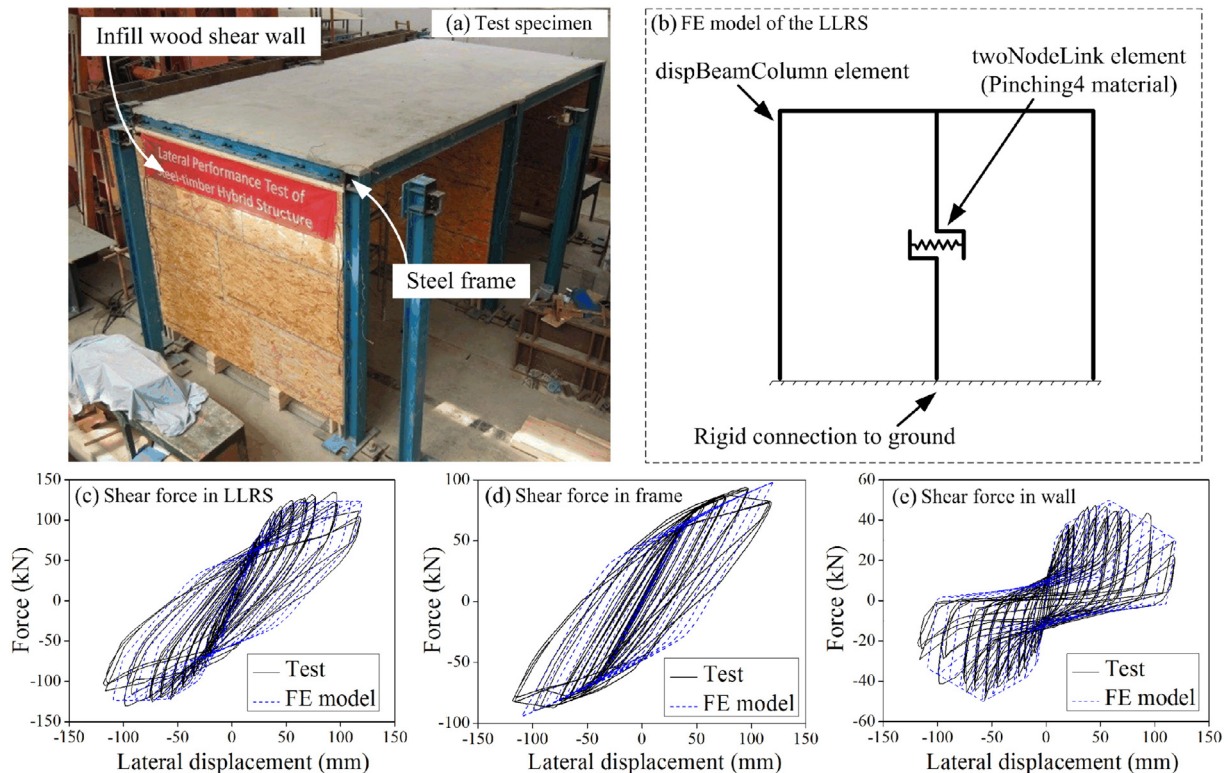
Fig. 5. FE model verification: (a) test specimen; (b) FE model of the LLRS; (c) shear force in LLRS; (d) shear force in frame; and (e) shear force in wall.
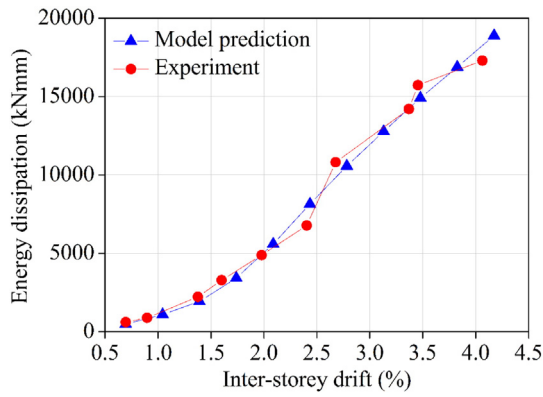
Fig. 6. Verification of cumulative energy dissipation.

of the load-displacement hysteresis and load sharing between the steel frame and infill wall were compared with test results, as shown in Fig. 5(c), 5(d), and 5(e). Moreover, the comparison between the model predictions of cumulative energy dissipation and those obtained from the test was also presented in Fig. 6. Good agreement between the test results and model predictions can be observed. Therefore, the model was further used to evaluate the seismic performance of the multi-story prototype structures.

5. Seismic performance assessment

The seismic performance of the prototype structures with different lateral stiffness ratios was evaluated with numerical simulations. The performance targets of the steel-timber hybrid LLRS were first defined according to existing provisions and pervious test observations, and then a suite of ground motions, scaled to match the design spectrum from a seismic prone zone in China, was used as the input for nonlinear time-history analyses. Failure probabilities, with regard to different hazard levels, were evaluated, and the wall-frame load sharing mechanism was also investigated.

5.1. Drift based performance targets

Inter-story deformation is usually a good indicator of structural or non-structural damage. For both the steel moment-resisting frame and the light wood frame shear wall, the expected response with a well-established correlation between local and global damage measures can be related to inter-story drift. The structural performance levels and illustrative damage for both the steel frame structures and light frame wood structures are provided in ASCE/SEI-41 [24]. The inter-story drift

Fig. 7. Experimental pushover response of the steel-timber hybrid LLRS.

limits for the steel moment-resisting frames were provided by a former version of ASCE/SEI-41 [25]; 0.7%, 2.5%, and 5.0% were defined as drift limits for the immediate occupancy (IO), life safety (LS), and collapse prevention (CP) performance levels, respectively. However, it seems that these drift limits are not conservative enough, especially for the CP performance level. Moreover, research programs have quantified the inter-story drift limits for light frame wood structures and similar structural systems, such as cold-formed steel structures. For light frame wood structures, Filiatrault and Folz [9] and Pang et al. [26] adopted 1.0%, 2.0%, and 3.0% as drift limits for the IO, LS, and CP performance levels, respectively. For cold-formed steel structures, Dubina [27] suggested different inter-story drift limits, corresponding to different performance levels as 0.3%, 1.5% and 2.5% for fully operational, partially operational, and ultimate limit states, respectively. Fiorino et al. [28] defined the inter-story drift limits for cold-formed steel structures based on the generic response curve from the result of a shear wall test. However, there are no code provisions for determining seismic performance targets and relative inter-story drift limits for the hybrid system with steel frames and infill wood shear walls. Hence, attempts were made to provide rational inter-story drift limits for the proposed structural systems based on previous test results and the damage descriptions in ASCE/SEI-41 [24]. Three performance levels including IO, LS, and CP were considered. The IO performance level is the post-earthquake damage state in which a structure remains safe to occupy, and little damage has occurred. This indicates that minor local yielding in a few steel members has occurred, and a few nail connection failures in the infill wood shear wall can be accepted. The LS performance level is defined as the post-earthquake damage state in which a structure has damaged components but retains a margin against onset of partial or total collapse. Moderate loosening of nail connections may occur in wood shear walls, and hinges may form in the steel members. The CP performance level is defined as the post-earthquake damage state in which the building is on the verge of partial or total collapse, which includes significant strength and stiffness degradation of the LLRS.

The lateral load resisting behavior of the steel-timber hybrid LLRS was obtained experimentally, as shown in Fig. 7. The y-axis of Fig. 7 is defined as V/V_{max}, where V is the shear force in the LLRS under the corresponding drift, and V_{max} is the maximum lateral load resisting capacity of the LLRS. Test results demonstrated that minor splitting of sheathing panel near corner nailed connections was initially observed under a drift ratio of 0.5%, and yielding of steel frame members was first observed under the drift ratio of 0.7%. Therefore, the drift ratio of 0.5% was a reasonable drift limit for the IO performance level in this study. As tests proceeded, damage accumulated in the nailed connections and yielding zone kept expending in the steel members. Many nail connection failures were observed in the sheathing corners under the drift ratio of 2.0%, but the structure still had sufficient stiffness and strength against the onset of partial or total collapse. When the drift ratio reached 3.0%, many nailed connections failed due to edge tear-out or fatigue fracture, and extensive yielding of the steel members was observed. Therefore, similar to the assumptions in Refs. [9,26], 2.0% and 3.0% were adopted as drift limits for the LS and CP performance levels, respectively.

5.2. Seismic input

According to CCSDB [16], a high seismic zone with design intensity VIII was assumed for this study. The soil condition was selected as type II, with an average shear wave velocity of the upper 30 m of the site profile (Vs30) between 280 m/s and 480 m/s, representing a very dense soil or stiff soil condition. Destructive historical earthquake records, most of which have similar soil conditions as the assumed site, were selected from the Pacific Earthquake Engineering Research Center's Next Generation Attenuation (NGA) database. The ground motion records used in this study are listed in Table 3.
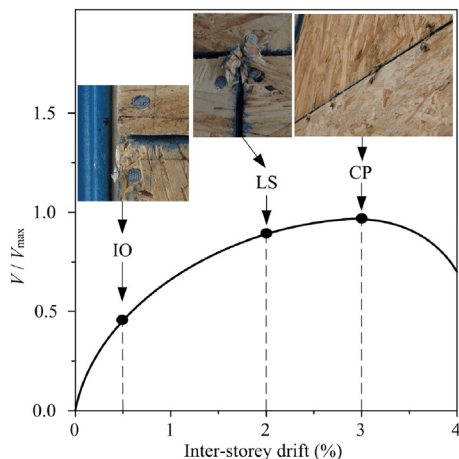
Table 3
Ground motion records used in analysis.

No.	Event	Time	Station	Component	PGA (g)	R_{JB} (km)	Magnitude	Vs30 (m/s)
1	Imperial Valley	1979.10.15	Cerro Prieto	CPE147	0.168	15.19	6.53	471.53
2	Imperial Valley	1979.10.15	Parachute Test Site	PTS225	0.113	12.69	6.53	348.69
3	Kern County	1952.07.21	Taft Lincoln School	TAF021	0.159	38.42	7.36	385.43
4	Tottori	2000.06.10	HRS021	EW	0.261	36.32	6.61	409.29
5	Northridge	1994.01.17	Moorpark-Fire Sta	MPR09	0.193	16.92	6.69	341.58
6	Northridge	1994.01.17	LA - Baldwin Hills	BLD090	0.239	23.50	6.69	297.07
7	Northridge	1994.01.17	Hollywood-Willoughby Ave	WIL090	0.136	17.82	6.69	347.7
8	San Fernando	1971.02.09	Santa Felita Dam	FSD172	0.155	24.69	6.61	389.00
9	Cape Mendocino	1992.04.25	Fortuna - Fortuna Blvd	FOR000	0.117	15.97	7.01	457.06
10	Cape Mendocino	1992.04.25	Eureka - Myrtle & West	EUR000	0.154	40.23	7.01	337.46
11	Chichi	1999.09.20	CHY046	EW	0.145	24.10	7.62	442.15
12	Chichi	1999.09.20	TCU046	EW	0.142	16.74	7.62	465.53
13	Chichi	1999.09.20	TCU056	EW	0.156	10.48	7.62	403.20
14	Chuetsu-oki	2007.07.16	Hinodecho Yoshida Tsubame City	NS	0.112	20.44	6.80	261.55
15	Chuetsu-oki	2007.07.16	NIGH1	NS	0.184	21.19	6.80	375.00
16	Iwate	2008.06.13	AKTH19	EW	0.164	32.28	6.90	287.96
17	Iwate	2008.06.13	Kami	NS	0.128	25.15	6.90	477.51
18	Darfield	2010.09.03	Canterbury Aero Club	EW	0.186	14.48	7.00	280.26
19	Darfield	2010.09.03	DFHS	EW	0.472	11.86	7.00	344.02
20	Darfield	2010.09.03	Riccarton High School	EW	0.190	13.64	7.00	293.00

In CCSDB [16], the 50-year exceedance probabilities for the earthquakes considered in the IO, LS and CP limit states were 63%, 10% and 2%, in accordance with the average return period of 50, 475, and 2475 years, respectively. The design spectrum, with respect to the considered seismic intensities and soil condition, were determined using the detailed provisions in CCSDB [16]. The plateau spectral accelerations corresponding to the IO, LS, and CP hazard levels were 0.16 g, 0.45 g, and 0.90 g, respectively. As listed in Table 4, the fundamental period of the elastic prototype structures ranged from 0.487 s to 1.408 s. To capture the structural responses over the entire range of periods, the historical earthquake excitations were matched to the design spectrum with the period range from $0.2T_{min}$ to $1.5T_{max}$, where T_{min} and T_{max} were, respectively, the smallest and largest periods among the nine prototype structures. Herein, the lower bound captured the higher modes of the elastic structure, and the upper bound captured the nonlinear response of the structure, once yielding and stiffness degradation occurs. The software package SeismoMatch [29] was used to conduct the matching using the wavelet algorithm proposed by Hancock et al. [30]. The matching criteria were that the spectrum of each ground motion with 5% damping should be always close to the design spectrum over the periods ranging from $0.2T_{min}$ to $1.5T_{max}$; however, 10%–15% fitting error was acceptable. Moreover, the average spectrum of the suite of ground motions should be above the design spectrum over the matching range. To create a seismic response database for the proposed structural system, nonlinear time-history analyses were performed at three spectral acceleration (S_a) levels (i.e., 0.16 g, 0.45 g, and 0.90 g), which corresponded to the IO, LS, and CP hazard levels. An example for the matching process for the CP hazard level is shown in Fig. 8.

6. Results and discussions

6.1. Fundamental periods

The lateral stiffness ratio λ has a crucial influence on the structural period. Structures with larger λ adopt stiffer infill wood shear walls

Table 4
Fundamental period of the prototype structures (units: s).

Lateral stiffness ratio λ	Number of stories		
	3	6	9
1:1	0.710	1.297	1.408
2:1	0.568	1.008	1.083
3:1	0.487	0.853	0.913

and have a lower period. On average, the period of the prototype structure decreased by 21.6% when λ increased from 1.0 to 2.0, and the period of the prototype structure decreased 15.0% more when λ further increased from 2.0 to 3.0. For all three considered building heights, Fig. 9 demonstrates the relationships between the fundamental period and λ.

6.2. Peak inter-storey drift response

The cumulative distribution function (CDF) is used to evaluate the probability of the structural drift response exceeding the performance criterion under a specific hazard level. The drift responses of the LLRS from nonlinear time-history analyses over the suite of earthquake ground motions were fit to a lognormal distribution, as given by Eq. (10):

$$F_x(x) = \Phi\left(\frac{(\ln x - \mu)}{\xi}\right) \tag{10}$$

where $\Phi()$ is the standard normal CDF; and μ and ξ are logarithmic distribution parameters, which are obtained by a maximum likelihood procedure. CDF curves can provide clear information on the expected performance at a given hazard level in a concise manner, and they are easily interpreted by design engineers. The CDFs for peak inter-story drift are shown in Fig. 10. The probability of failure with respect to a specified hazard level can be evaluated by the CDF, given the performance criterion. As expected, as the parameter λ increases, the peak
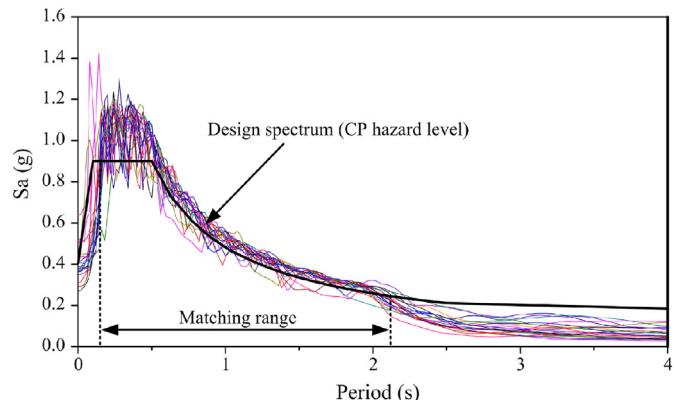
Fig. 8. Ground motion records matched to the design spectrum for CP hazard level.
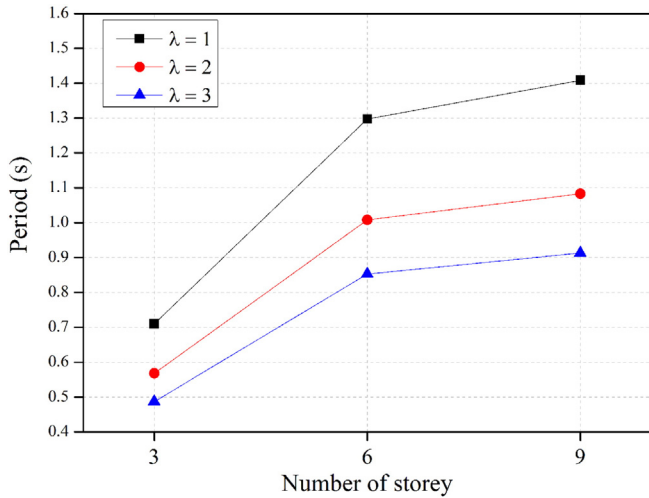
Fig. 9. Fundamental period of the prototype structures.

drift response of the LLRS decreases. For instance, given the drift limit of 3.0% under the CP performance level, the failure probabilities for the 3-storey structure with λ equal to 1.0, 2.0, and 3.0 are 47.7%, 7.4%, and 0.1%, respectively. The failure probability was reduced significantly when stronger infill walls were used, even under earthquake excitations with a return period of 2475 years. For the LS performance level, the peak inter-story drift responses of the prototype structures are much smaller than the specified drift limit (i.e., 2%), indicating limited stiffness degradation of the infill wood shear wall under earthquake excitations. Thus, the performance-based design of the proposed steel-timber hybrid structural system can focus on sizing the steel and timber members to have sufficient elastic stiffness under the IO performance level and to maintain reasonable post-yielding stiffness under the CP performance level.

6.3. Loading sharing between steel frame and wood shear wall

The lateral load distribution between the steel frame and wood shear wall is represented by a load sharing parameter κ, which is
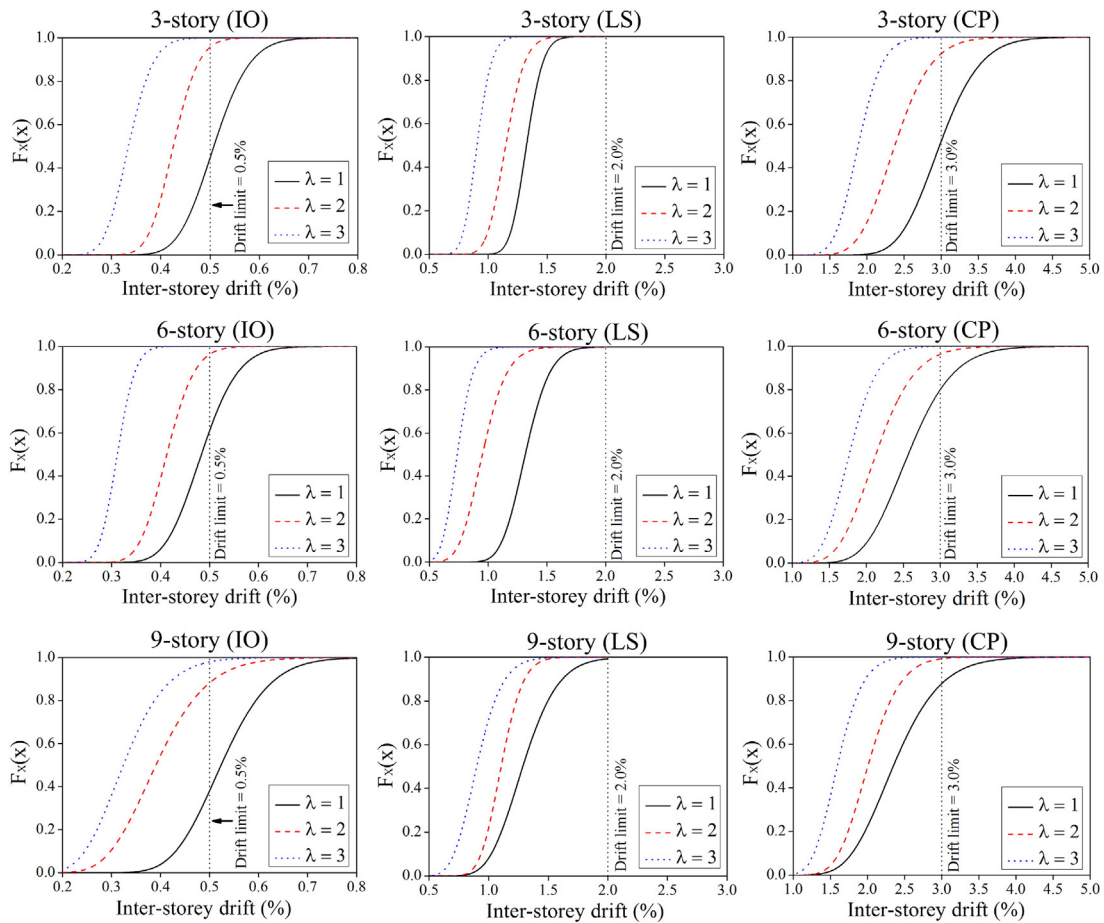
Fig. 10. Cumulative peak drift distributions.
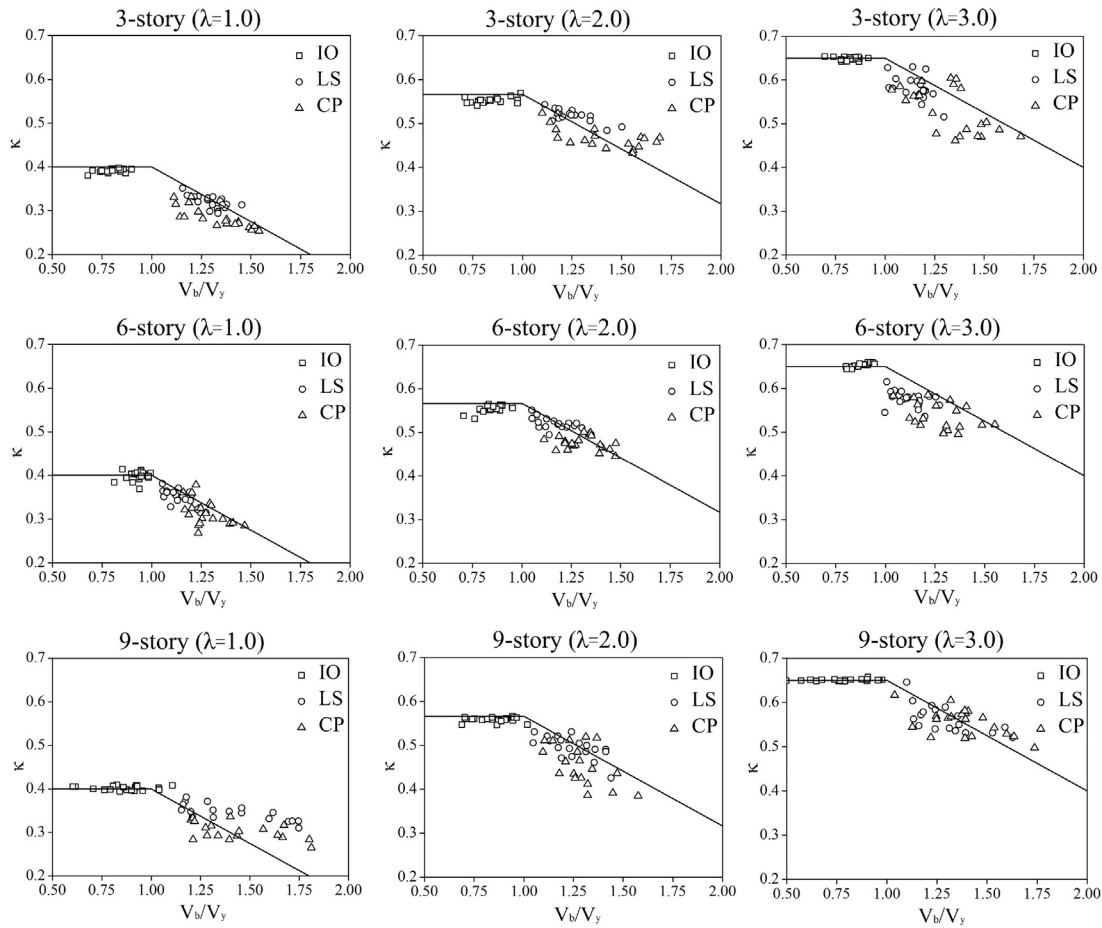
Fig. 11. Load sharing parameter κ in steel-timber hybrid LLRS.

calculated by Eq. (11):

$$\kappa = \frac{V_{wood}}{V_{wood} + V_{steel}} \tag{11}$$

where V_{wood} is the lateral load resisted by the infill wood shear wall, and V_{steel} is the lateral load resisted by the steel frame. To investigate the variation of κ with respect to the IO, LS, and CP performance levels, the lateral load resisted by the infill wood shear wall and that resisted by the steel frame were recorded with nonlinear time-history analyses. Both the total base shear and lateral stiffness ratio, λ, had significant influence on the magnitude of κ. Fig. 11 demonstrates the load sharing parameter κ for each prototype structure. The horizontal axis represents the ratio as V_b/V_y. Here, V_b is the base shear of the structure corresponding to the maximum inter-story drift state under a specific earthquake excitation and can be directly obtained from the time-history analysis, and V_y is the yield base shear of the structure obtained from a pushover analysis. In Fig. 11, one data point represents the result from one time-history analysis. Interestingly, the relationship between κ and V_b/V_y follows a similar trend in all nine prototype structures. κ almost remained constant when V_b/V_y was smaller than 1.0, and κ started to decrease when the base shear was larger than V_y. Thus, Eq. (12) is proposed to estimate the value of κ:

$$\kappa = \left\{ \begin{array}{ll} \gamma/(\gamma+1)-0.1 & \text{when } V_b/V_y \leq 1.0 \\ \gamma/(\gamma+1)-0.25 \times (V_b/V_y-1.0)-0.1 & \text{when } V_b/V_y > 1.0 \end{array} \right\} \tag{12}$$

Eq. (12) is plotted as a bilinear line in Fig. 11. The proposed equation provided a reasonable estimation of the wall-frame load sharing

mechanism, and for most cases, it represented an average value of κ from the suite of earthquake excitations.

6.4. Non-structural damage

Earthquake induced non-structural damage is also considered to be an important performance indicator, especially for performance-based design. The damage state criteria for drift-sensitive and acceleration-sensitive non-structural components are specified in earthquake loss estimation methodology (HAZUS-MH MR5) [31]. Damage to drift-sensitive non-structural components (e.g., full-height drywall partitions) is primarily a function of inter-story drift, while for acceleration-sensitive components (e.g., mechanical equipment), damage is normally a function of the floor acceleration. Table 5 provides the median peak inter-story drift ratios and peak floor accelerations as performance criteria for non-structural damage in accordance with Ref. [31]. Four non-structural damage states are considered: slight, moderate, extensive, and complete. Detailed descriptions of the damage states for various non-structural components can be found in Ref. [31]. Slight damage can be considered fully

Table 5
Performance criteria for non-structural damage.

Category	Non-structural damage states			
	Slight	Moderate	Extensive	Complete
Drift limit for drift-sensitive non-structural components	0.4%	0.8%	2.5%	5.0%
Floor acceleration limit for acceleration-sensitive non-structural components	0.3 g	0.6 g	1.2 g	2.4 g
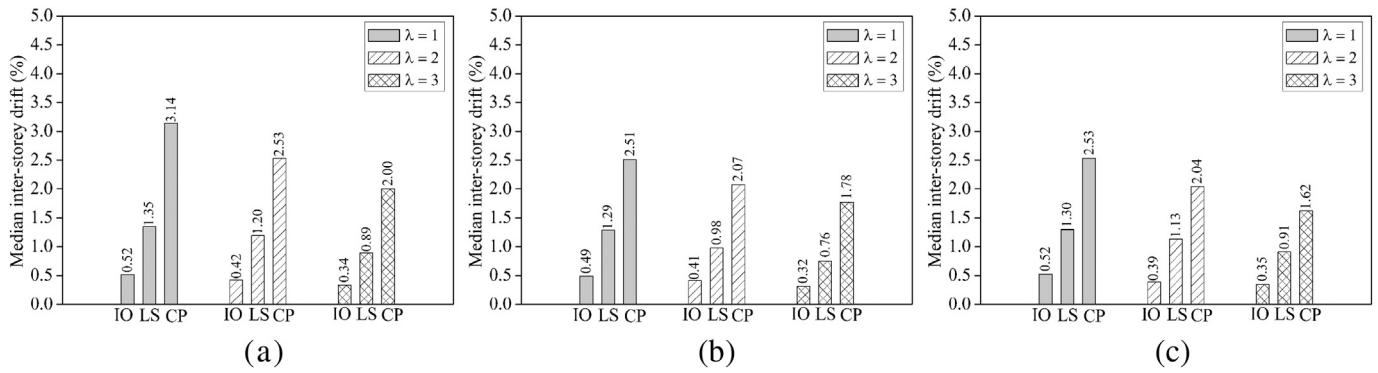
Fig. 12. Inter-story drift response of the prototype structures (a) 3-story; (b) 6-story; and (c) 9-story.

operational, which is expected for the IO performance level. However, the LS performance level may be associated with moderate to extensive non-structural damage, and the CP performance level may be associated with extensive to even complete non-structural damage.

Fig. 12 demonstrates the median peak inter-story drifts of the prototype structures. For drift-sensitive non-structural components, slight damage is expected under the seismic excitation corresponding to IO performance level for almost all prototype structures, while moderate to extensive damage of non-structural components is expected for most cases under both LS and CP performance levels, which provides inter-story drift ranging from 0.76% to 2.07%. However, extensive to complete damage of non-structural components is expected for four cases (i.e., 3-story building with λ equal to 1.0 and 2.0 under CP, 6-story building with λ equal to 1.0 under CP, and 9-story building with λ equal to 1.0 under CP).

Fig. 13 demonstrates the peak floor accelerations of the prototype structures. The peak floor accelerations of all prototype structures under the seismic excitation corresponding to the IO performance level were less than the performance criterion for slight damage states (i.e., 0.4 g), indicating very little damage for acceleration-sensitive non-structural components under the IO performance level. Moderate damage of non-structural components was expected for all prototype buildings under the LS performance level, while extensive damage of non-structural components was expected under the CP performance level. For non-structural components, the drift-induced damage was more significant than the acceleration-induced damage, especially under the CP performance level. This was primarily due to the stiffness degradation of the infill wood shear wall, which increased the period of the structure, further decreasing the acceleration response.

6.5. Residual deformation

Current seismic design philosophies emphasize the importance of designing ductile structural systems to undergo inelastic deformation under earthquakes, while sustaining their integrity. In performance-based design approaches, the performance of a structure is normally assessed based on the maximum transient inter-story drift during the earthquake. Past earthquake observations demonstrated that residual deformation is almost inevitable in a design-level earthquake event. As stated by Christopoulos et al. [32], residual deformations can result in the partial or total loss of a building if static incipient collapse is reached and if the structure appears unsafe to occupants. Moreover, the magnitude of residual deformation is closely related to the repair cost of a building. McCormick et al. [33] observed that it is not normally economical to repair a building with a residual inter-story drift larger than 0.5%. This section provides a residual drift assessment on the steel-timber hybrid structural system. To obtain residual drifts from nonlinear time-history analyses, a five-second vibration with a very small amplitude (i.e., 1.0 mm/s^2) was added to the end of each input earthquake excitation, and the drift response from this vibration was obtained as the residual drift of the structure. This five-second vibration was used to allow the structure to come to a complete rest before recording residual displacement, which was suggested by Ref. [32].

The average residual drift under each performance level was plotted in Fig. 14. For all prototype structures, the residual drifts ranged from 0.03% to 0.10% after earthquake excitations corresponding to the IO performance level, while the residual drift ranged from 0.11% to 0.22% after earthquake excitations corresponding to the LS performance level. With a residual drift far less than 0.5%, it will be economical to restore the functionality of the structure after repair and rehabilitation. The residual drift of the structures with λ equal to 1.0 and 2.0 under the CP performance level was between 0.57% and 0.97%, which indicated that the repair cost may be very high; thus, it may be more economical to demolish the building and build a new one. However, if strong infill wood shear walls are adopted in the hybrid structure (such as λ = 3.0), the residual drifts of the structures under the CP performance level were significantly reduced to approximately 0.4%, which may greatly reduce repair costs.
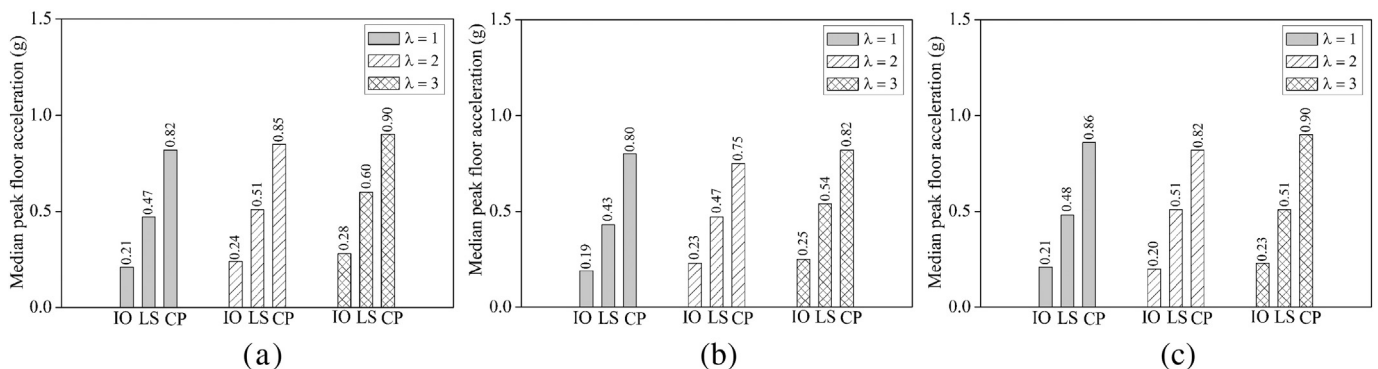
Fig. 13. Floor acceleration response of the prototype structures (a) 3-story; (b) 6-story; and (c) 9-story.
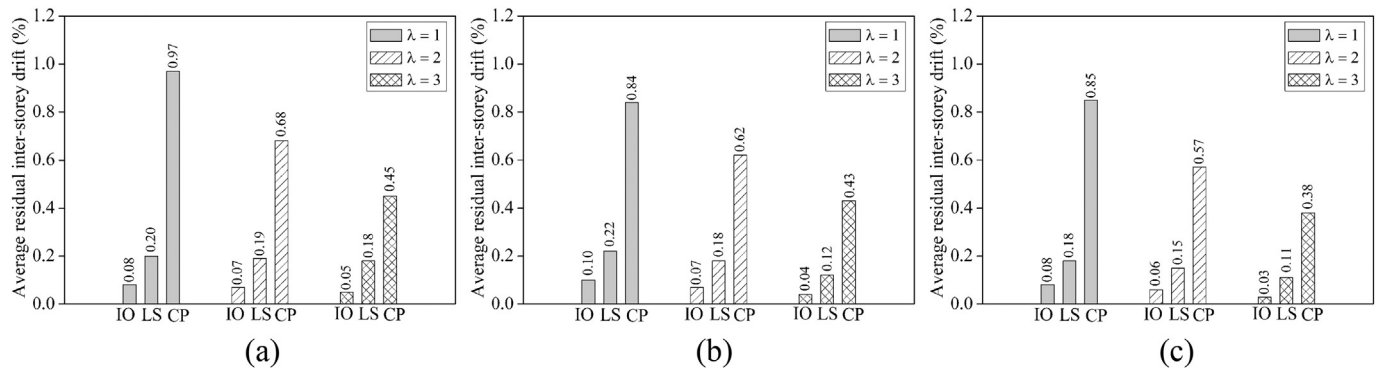
Fig. 14. Residual drift of the prototype structures (a) 3-story; (b) 6-story; and (c) 9-story.

7. Summary and conclusions

A steel-timber hybrid building made of steel moment-resisting frames and prefabricated infill wood shear walls to resist later loads for multi-story buildings has been proposed. This paper presents a seismic performance assessment for these hybrid structures. The performance-based seismic design objectives under the IO, LS, and CP performance levels were discussed and defined. Nine prototype structures with three building height levels (i.e., 3-story, 6-story, and 9-story) and various infill wall configurations were designed. The infill configurations were designed based on the lateral infill-to-frame stiffness ratio, λ. FE models were developed for the steel-timber hybrid structures, and comprehensive nonlinear time-history analyses were conducted to investigate the seismic behavior of the prototype structures.

The lateral stiffness ratio, λ, crucially influenced the fundamental period of the structure. Since the structure with large λ adopted stiffer and stronger infill wood shear walls, the period of the prototype structure decreased by 21.6%, on average, when λ increased from 1.0 to 2.0, and the period of the prototype structure decreased further by 15.0% when λ increased from 2.0 to 3.0. The probability of failure, with respect to a specified hazard level, was evaluated on the CDF given the performance criterion. As expected, as λ increased, the shear wall peak displacement decreased. The results demonstrated that the drift targets for the LS performance level did not control the design of the LLRS of the steel-timber hybrid structure. Thus, the performance-based design of the proposed steel-timber hybrid structural system should be focused on sizing the steel and timber members to have sufficient elastic stiffness under the IO performance level and maintaining a reasonable amount of post-yielding strength and stiffness under the CP performance level. The post-yield behavior was closely related to the lateral wall-frame load sharing mechanism in the hybrid structure. A load sharing parameter was defined to describe the lateral force distribution among the frame and the infill wall, and a formula was proposed by fitting the time-history analytical results to estimate the load sharing parameter.

Non-structural damage was also considered in the performance assessment. It is noted that drift-induced damage on non-structural elements was more significant than the acceleration-induced damage, especially under the CP performance level. Moreover, the maximum residual drifts from each nonlinear time-history analysis were extracted, and the average residual drift under each performance level was reported. The results indicated that for hybrid prototype structures, the average residual drift was acceptable under both IO and LS performance levels. However, excessive residual drift was observed for prototype structures with λ equal to 1.0 or 2.0 under the CP performance level. If stiffer infill wood shear walls were adopted (such as λ equal to 3.0), the residual drifts of the structure under CP performance level could be significantly decreased to a more acceptable level.

This study provided insights and suggestions for performance-based seismic design of a steel-timber hybrid structural system, and the results from the time-history analyses can serve as a technical basis for evaluating the post-yielding behavior of the steel-timber hybrid structure, considering the nonlinear wall-frame load sharing effect.

References

[1] D. Wu, Y. Xiong, P. Tan, Research on the application of information system to damage of buildings in Wenchuan county town during the Wenchuan earthquake, 2nd IEEE International Conference on Information Management and Engineering (IEEE), ICIME2010, Chengdu, China, 2010.

[2] S.H. Potter, J.S. Becker, D.M. Johnston, K.P. Rossiter, An overview of the impacts of the 2010–2011 Canterbury earthquakes, Int J Disaster Risk Reduct 14 (2015) 6–14.

[3] M. He, Z. Li, F. Lam, R. Ma, Z. Ma, Experimental investigation on lateral performance of timber-steel hybrid shear wall systems, J. Struct. Eng. ASCE 140 (6) (2014) (04014029-1-12).

[4] Z. Li, M. He, Z. Ma, K. Wang, R. Ma, In-plane behavior of timber-steel hybrid floor diaphragms: experimental testing and numerical simulation, J Struct Eng ASCE 142 (12) (2016) (04016119-1-14).

[5] S. Tesfamariam, S.F. Stiemer, C. Dickof, M.A. Bezabeh, Seismic vulnerability assessment of hybrid steel-timber structure steel frame with CLT infill, J. Earthq. Eng. 18 (6) (2014) 929–944.

[6] C. Dickof, S.F. Stiemer, M.A. Bezabeh, S. Tesfamariam, CLT-steel hybrid system: ductility and overstrength values based on static pushover analysis, J. Perform. Constr. Facil. 28 (6) (2014) (A4014012).

[7] X. Zhang, M. Fairhurst, T. Tannert, Ductility estimation for a novel timber-steel hybrid system, J. Struct. Eng. ASCE 142 (4) (2016), E4015001. (-1-11).

[8] A.S.C.E/.S.E.I. 7-10, Minimum Design Loads for Buildings and Other Structures, ASCE, Reston, VA, 2010.

[9] A. Filiatrault, B. Folz, Performance-based seismic design of wood framed buildings, J. Struct. Eng. ASCE 128 (1) (2002) 39–47.

[10] J.W. van de Lindt, S.E. Pryor, S. Pei, Shake table testing of a full-scale seven-story steel-wood apartment building, Eng. Struct. 33 (3) (2011) 757–766.

[11] S.C. Goel, S.H. Chao, Performance-based Plastic Design: Earthquake-resistant Steel Structures, Washington, USA, International Code Council, 2009.

[12] H. Akiyama, Earthquake-Resistant Limit-state Design of Buildings, University of Tokyo Press, Tokyo, Japan, 1985.

[13] S.H. Chao, S.C. Goel, S.S.A. Lee, Seismic design lateral force distribution based on inelastic state of structures, Earthquake Spectra 23 (3) (2007) 547–569.

[14] S. Kharmale, S. Ghosh, Performance-based plastic design of steel plate shear walls, J. Constr. Steel Res. 90 (2013) 85–97.

[15] Chinese Standard GB 50017, Code for design of steel structures, National Standard of the People's Republic of China (NSPRC), Beijing, China (in Chinese), 2003.

[16] Chinese Standard GB 50011, Code for seismic design of buildings, National Standard of the People's Republic of China (NSPRC), Beijing, China (in Chinese), 2010.

[17] Chinese Standard GB 50005, Code for design of timber structures, National Standard of the People's Republic of China (NSPRC), Beijing, China (in Chinese), 2003.

[18] American Society for Testing and Materials (ASTM) F1667, Standard Specification for Driven Fasteners: Nails, Spikes, and Staples. West Conshohocken, USA, 2015.

[19] Z. Li, M. He, F. Lam, M. Li, Load-sharing mechanism in timber-steel hybrid shear wall systems, Front. Struct. Civ. Eng. 9 (2) (2015) 203–214.

[20] McKenna F, G.L. Fenves, M.H. Scott, B. Jeremic, Open system for earthquake engineering simulation (OpenSees), Rep. Prepared for the Pacific Earthquake Engineering Research Center, College of Engineering, Univ. of California, Berkeley, CA, 2000.

[21] J.P. Judd, F.S. Fonseca, Analytical model for sheathing to framing connections in wood shear walls and diaphragms, J. Struct. Eng. ASCE 131 (2) (2005) 345–352.

[22] J. Xu, J.D. Dolan, Development of nailed wood joint element in ABAQUS, J. Struct. Eng. ASCE 135 (8) (2009) 968–976.

[23] Z. Li, M. He, F. Lam, M. Li, R. Ma, Z. Ma, Finite element modeling and parametric analysis of timber-steel hybrid structures, Struct Des Tall Spec 23 (14) (2014) 1045–1063.

[24] ASCE/SEI-41, Seismic Evaluation and Retrofit of Existing Buildings, ASCE, Reston, VA, 2013.

[25] ASCE/SEI-41, Seismic Rehabilitation of Existing Buildings, ASCE, Reston, VA, 2006.

[26] W. Pang, D. Rosowsky, S. Pei, J.W. van de Lindt, Simplified direct displacement design of six-story woodframe building and pretest seismic performance assessment, J. Struct. Eng. ASCE 136 (7) (2010) 813–825.

[27] D. Dubina, Behaviour and performance of cold-formed steel-framed houses under seismic action, J. Constr. Steel Res. 64 (2008) 896–913.

[28] L. Fiorino, O. Iuorio, V. Macillo, R. Landolfo, Performance-based design of sheathed CFS buildings in seismic area, Thin-Walled Struct. 61 (2012) 248–257.

[29] Seismosoft. Seismomatch v2.1-A computer program for spectrum matching of earthquake records. http://www.seismosoft.com, 2016.

[30] J. Hancock, J. Watson-Lamprey, N.A. Abrahamson, J.J. Bommer, A. Markatis, E. Mccoy, R. Mendis, An improved method of matching response spectra of recorded earthquake ground motion using wavelets, J. Earthq. Eng. 10 (S1) (2006) 67–89.

[31] HAZUS-MH MR5, Earthquake loss estimation methodology, Technical and User's Manual, Department of Homeland Security, FEMA, Mitigation Division, Washington D.C., 2010.

[32] C. Christopoulos, S. Pampanin, N. Priestley, Performance-based seismic response of frame structures including residual deformations. Part I: single-degree of freedom systems, J. Earthq. Eng. 7 (1) (2003) 97–118.

[33] J. McCormick, H. Aburano, M. Ikenaga, M. Nakashima, Permissible residual deformation levels for building structures considering both safety and human elements, Proc 14th World Conf Earthquake Engineering, Seismological Press of China, Beijing, 2008 Paper ID 05-06-0071.